Hybrid hierarchical homogenization theory for unidirectional CNTs-coated fuzzy fiber composites undergoing inelastic deformations

Qiang Chen, George Chatzigeorgiou, Fodil Meraghni *

Arts et Métiers Institute of Technology, CNRS, Université de Lorraine, LEM3-UMR7239, F-57000 Metz, France

A B S T R A C T

A new hybrid homogenization approach is proposed for simulating the homogenized and local response of unidirectional fuzzy fiber nanocomposites undergoing inelastic deformations. Fuzzy fiber composites are hierarchical reinforcing structures where the fibers coated with radially aligned carbon nanotubes (CNTs) are embedded in the matrix. In this spirit, the fuzzy fiber composites are modeled as a three-scale medium. At the microscale, the CNTs-reinforced matrix is homogenized as nanocomposite interphase (NCP) attached to the main fiber via the asymptotic expansion homogenization (AEH). At the mesoscale, an intermediate equivalent fiber that substitutes for the NCP and the main fiber is constructed using the composite cylinder assemblage (CCA) and the transformation field analysis (TFA) techniques. At the macroscale, homogenization of the equivalent fiber and the surrounding matrix is handled by AEH which yields the effective response of the whole fuzzy fiber composites. The new technique facilitates accurate and efficient studies of the inelastic deformation mechanisms of periodic fuzzy fiber arrays with single or multiple inclusions under biaxial and triaxial loading conditions, eliminating exhausting interphase mesh discretizations encountered in the classical full-field homogenization. An added advantage is that the proposed theory captures the fiber-fiber interaction neglected in the classical CCA-TFA, an issue that leads to the exceptionally stiff post-yielding stress-strain response common in the mean-field micromechanics approaches.

1. Introduction

Carbon nanotubes have been demonstrated to be a promising candidate material for enhancing the mechanical and physical properties of the traditional fiber-reinforced polymer composites, especially for improving the interfacial and transverse mechanical properties [1–5]. This scientific interest is motivated by the fact that CNTs have an axial Young's modulus ranging between 300 and 1000 GPa, while their theoretical elongation to break reaches 30–40% [6–8]. Particularly, grafting or depositing CNTs on the fiber surfaces through the chemical vapor deposition [9] and electrospray technique [10], etc., to form the fuzzy fiber reinforcements, is one of the most favorable techniques. In essence, composites with enhanced fibers are hierarchical reinforcing structures, in which the glass or ceramic fibers are coated with CNTs, and the latter is embedded in the polymer matrix, as depicted in Fig. 1 by Li et al. [11] and Aziz et al. [12].

Thus far, much effort has been made to validate the effectiveness of the CNTs-reinforced interphase in improving the interfacial and mechanical properties of such composites, for instance, the interfacial damage [11–13], tensile modulus [11], toughness [14], and energy absorption [3]. Apart from the experimental investigation, the increasing usage and development of new fuzzy fiber composites and their structural components have also flourished a novel research sphere from the simulation communities aiming at identifying the nano/microstructure-property relationship of such composites. On account that the CNTs are deposited on the surface of the main fiber in all the possible radial directions, the interlayer is often viewed as a homogenous equivalent medium with cylindrically orthotropic properties. As such, the fuzzy fiber composites can be modeled as two concentric cylinders placed in the matrix phase, producing a three-scale medium with micro-(CNTs reinforced matrix), meso-(fuzzy fiber-reinforced matrix), and macro-(composites) scales.

Homogenization of the hierarchical media requires appropriate reiterated homogenization methods such as [15]. Broadly speaking, two groups of approaches have been adopted in the literature for predicting the effective behavior of fuzzy fiber composites with micromechanics simulations. The first group of approaches includes mainly the classical micromechanics approaches that contain either no detailed

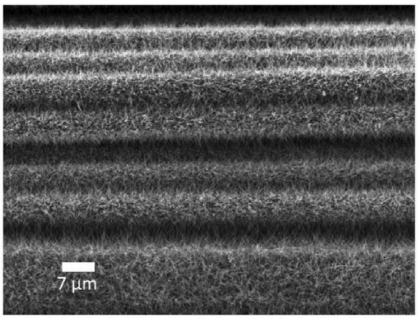

(a)

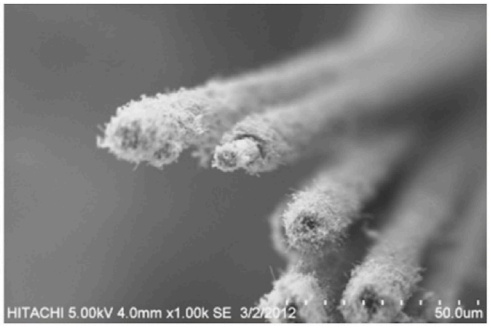

(b)

Fig. 1. Scanning electron microscopy image of fibers with densely-packed CNTs on the surface by (a) Li et al. [11] and (b) Aziz et al. [12]. Fig. 1(a) is reprinted from the Composite Science and Technology, Vol. 117, "Hierarchical carbon nanotube carbon fiber unidirectional composites with preserved tensile and interfacial properties" by Richard Li, Noa Lachman, Peter Florin, H. Daniel Wagner, Brian L.Wardle, p139-145, 2015, with permission from Elsevier. Fig. 1(b) is reprinted from the Polymer Composites, Vol. 36, "Experimental evaluation of the interfacial properties of carbon nanotube coated carbon fiber reinforced hybrid composites" by Shazed Aziz, Suraya Abdul Rashid, Saeed Rahmanian et al., p1941-1950, 2015, with permission from John Wiley and Sons.

microstructural information, such as the Mori-Tanaka micromechanics strategy [16–19], or certain geometric representation of the material microstructure, such as the composite cylinder assemblage model [20–22]. Analytical solutions for the displacement and stress field in the presence of a cylindrically orthotropic interphase layer in unidirectional composites have been developed by Tsukrov and Drach [23]. Classical micromechanics approaches provide closed-form solutions for combined thermo-mechanical multiaxial loading, hence remain useful tools for the prediction of the effective behavior of heterogeneous materials. Nonetheless, the classical micromechanics approaches either neglect the interaction of the adjacent reinforcements or account for this interaction only in an average sense. Such interaction is crucial and its neglect may significantly underestimate the local stress fields that affect the damage and plastic field evolution. For instance, it is a well-known issue that the Mori-Tanaka approach predicts exceptionally high initial yielding strength and stiff post-yielding stress-strain response for composites. This overestimation is typically attributed to the lack of fiber-fiber interaction [16,24]. An advanced computational model based on the bridging micromechanics [25], developed originally by Huang [26,27], has also been applied to identify the effective properties of fuzzy fiber-reinforced composites.

Alternative approaches are based on the full-field displacement representation of repeating microstructures, commonly referred to as the repeating unit cell (RUC), with periodic displacement/traction boundary conditions. The finite-element [28–30] and finite-volume [31–33] methods in their various forms are the dominant techniques because of the ability to admit complex unit cell structures containing random inclusions of arbitrary shapes and sizes. They also permit the incorporation of arbitrary deformation mechanisms at the individual phase, such as plasticity [34], viscoelasticity-viscoplasticity [35,36], martensitic transformation [37], as well as hyperelasticity in finite transformation [38]. For the case of a continuous fuzzy fiber-reinforced composite, the effective properties have been determined by Kundalwal and Ray [19,39] using the method of cells approach and the finite element method. These numerical methods, however, require substantial mesh discretization to predict the drastically changing stress fields within the repeating unit cell in the case of plastic deformation. This is particularly true for the fuzzy fiber composites, in which the nanocomposite interphase presents spatially-dependent mechanical behavior in the Cartesian coordinates. Extensive mesh refinements in the affected region are preferred to capture the rapid variation of interphase properties. The elasticity-based locally-exact homogenization theory (LEHT) developed by Pindera and his coworkers [40,41] is a viable alternative to the prevalent finite-element and finite-volume-based micromechanics theories. The LEHT satisfies exactly the governing differential equations as well as the interfacial continuity conditions. The recent development of the LEHT provides a paradigm shift by admitting multi-inclusion random distribution for unidirectional composites [42]. In addition to the physics-based analytical or numerical techniques, machining learning-driven numerical approaches have also shown potential in the multiscale simulations of composite materials. The latter provides possible speed-ups of several magnitudes relative to the former ones [43,44].

To the best of the authors' knowledge, the effect of CNTs-reinforced interphase on the elastic properties is well documented in the literature through the classical micromechanics approaches and the periodic homogenization theories, whereas the effect of the CNTs-reinforced interphase on the elastoplastic response has not been investigated as extensively. Towards this end, a novel hybrid multiscale homogenization approach is constructed herein to predict reliably the response of fuzzy fiber composites. The new approach makes use of the CCA and the transformation field analysis approach recently developed by the present authors, Chatzigeorgiou et al. [20], as well as the periodic homogenization theory. Specifically, an intermediate equivalent fiber is obtained via the CCA-based TFA analysis. The equivalent fiber as a whole is a substitute for the fiber and nanocomposite interphase in the classical full-field homogenization. The significance of the hybrid homogenization is several-fold. First of all, the new approach avoids the exhausting interphase mesh discretization in the classical periodic homogenization, a substantial advantage especially in the case involving multiple inclusions of random distribution. Elimination of interphase mesh discretization also facilitates the simulating nanocomposite interphase of arbitrary thickness for understanding the influence of local properties and their microstructures on the macroscopic behavior over a large parameter space, thereby accelerating the development cycle of a material system for specific high-potential applications. The ability to capture the fiber-fiber interaction neglected in classical micromechanics is an added advantage of the hybrid homogenization. In this regard, the inelastic deformation mechanism can be described correctly using this new technique. The new contributions include:

- the first time that a hybrid hierarchical homogenization scheme is proposed for investigating the inelastic response of fuzzy fiber composites.
- demonstration that the new approach doesn't predict excessively stiff stresses inherent to the classical CCA-TFA homogenization, with the accuracy of the predicted local and global response comparable to the full-field homogenization.
- demonstration that the special strength of the hybrid hierarchical homogenization lies in the elimination of the three-dimensional mesh discretization of the nanocomposite interphase since the interphase and main fiber can be treated as an equivalent medium using an analytical approach.

The rest of the paper is organized as follows : Section 2 presents the theoretical framework of the new hybrid homogenization technique.

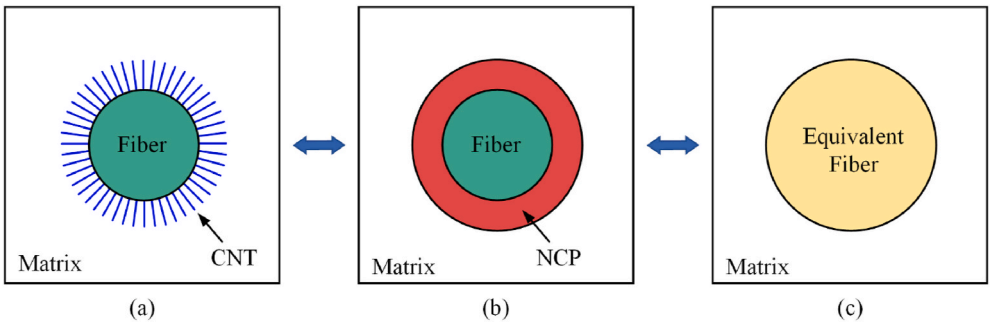

Fig. 2. (a) Microscale fuzzy fiber composites containing the main fiber, CNTs, and matrix phases; (b) Mesoscale fuzzy fiber composites containing the main fiber, nanocomposite interphase, and matrix; (c) Equivalent repeating unit cell containing equivalent fiber and matrix.

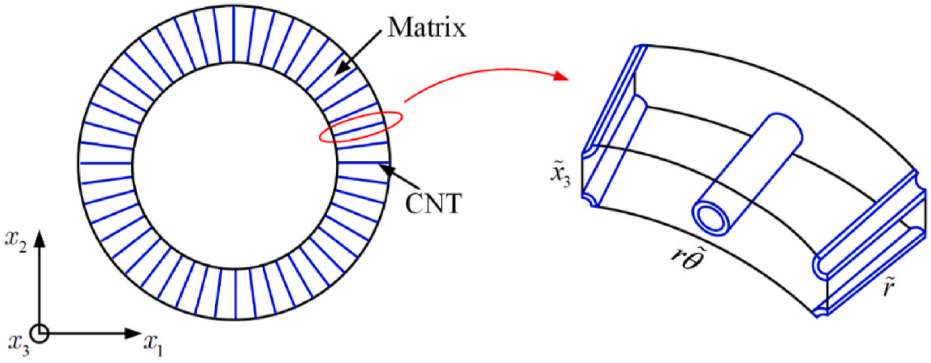

Fig. 3. Cross-section of the nanocomposite interphase.

Section 3 illustrates the new theory's capability to capture the homogenized and the local response of unidirectional fuzzy fiber composites with single inclusion vis-à-vis the classical periodic homogenization method and the CCA-TFA approach, under various uniaxial loadings. Numerical experiments conducted in Section 4 demonstrate the new approach's accuracy to capture the inelastic deformation mechanism under nonproportional loading paths. New results are also generated in order to highlight the strengths of the developed theory for simulating periodic multi-inclusion fuzzy fiber arrays. Section 5 draws pertinent conclusions leading to potential future work.

2. Theoretical framework

Fig. 2(a) depicts a repeating unit cell representing the geometrical characteristics of unidirectional fuzzy fiber composites. The main fibers are coated with radially oriented carbon nanotubes, which are further embedded in the matrix phase. Therefore, the fuzzy fiber composites can be treated as a three-phase medium comprised of the homogeneous main fiber, the matrix, and the nanocomposite interphase, Fig. 2(b). The latter is considered as an equivalent heterogeneous medium consisting CNTs (or microfibers) embedded in the matrix materials.

Accordingly, the multiscale homogenization approach proposed herein for such medium consists of three steps. The first step (microscale) is conducted on the nanocomposite interphase, where the CNTs-reinforced matrix is homogenized as an equivalent heterogeneous coating layer attached to the main fibers. The second homogenization step (mesoscale) is performed on the fuzzy fiber, in which a new equivalent fiber mimicking the inelastic response of the coated main fiber is obtained through a cylindrical representative volume element described in detail in the relevant subsection. Homogenization of the equivalent fiber and the remaining matrix at the macroscopic scale yields the overall constitutive relations of the fuzzy fiber composites, as illustrated in Fig. 2(c). It should be noted that the CNTs are assumed to have the same averaged radii and lengths. The effects of waviness [20] and irregular distribution patterns of the CNTs are not taken into account in this work.

2.1. Microscale: homogenization of nanocomposite interphase

Fig. 3 shows the microscopic cross-section of the nanocomposite interphase. It consists of radially aligned carbon nanotubes distributed uniformly in the matrix phase. The cylindrical structure of the nanocomposite interphase produces a challenge in terms of periodic homogenization in the Cartesian coordinate system since such structure cannot be replicated by repetition of the same unit cell, cf., Tsalis et al. [45,46]. An additional complication related to the cylindrical periodicity is the fact that the volume fractions of CNTs inside the surrounding matrix are reduced progressively with the increasing radial coordinates.

To properly capture the mechanical properties of the equivalent nanocomposite interphase medium, the asymptotic expansion homogenization approach, developed in the cylindrical coordinates by Chatzigeorgiou et al. [29], is utilized herein. The AEH provides a consistent framework for taking into account the effect of macroscopic strain variations in Cartesian/cylindrical periodic materials whose microstructural scale is characterized by the characteristic length δ [47,48]. In the cylindrical coordinates, the mesoscale coordinates are defined as (r,θ,x_3) and the microscale coordinates are defined as $(r/\delta,\ \theta/\delta,\ x_3/\delta)\rightarrow(\tilde{r},\tilde{\theta},\tilde{x}_3)$. For the sake of simplicity, the axes (r,θ,x_3) are denoted as $(1,2,3)$ as well. Within this framework, the macroscopic behavior of the composites is obtained when the microstructure length becomes infinitesimally small ($\delta\rightarrow 0$). The two-scale displacement field is represented by an asymptotic expansion in powers of δ:

$$\widehat{u}_i^{\delta}=\widehat{u}_i^{(0)}(r,\theta,x_3)+\delta\widehat{u}_i^{(1)}\left(r,\theta,x_3,\tilde{\theta},\tilde{x}_3\right)+\delta^2\widehat{u}_i^{(2)}\left(r,\theta,x_3,\tilde{\theta},\tilde{x}_3\right)+\cdots \tag{1}$$

where $\widehat{u}_i^{(0)}$ denotes the mesoscale displacement and $\widehat{u}_i^{(\delta)}$ are the periodic functions indicating the displacement fluctuations induced by the het-

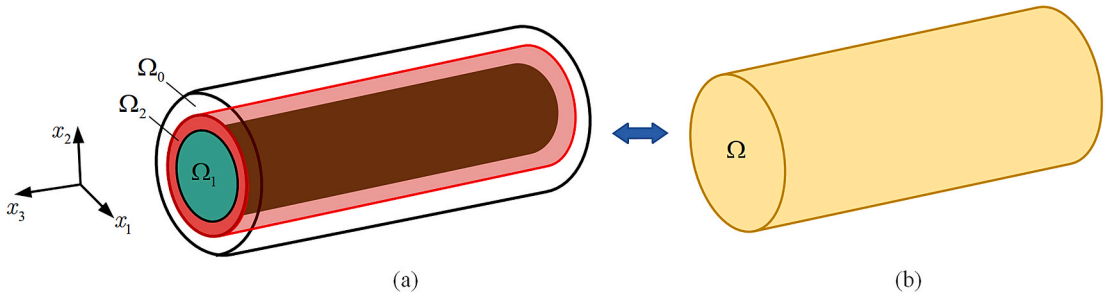

Fig. 4. (a) Composite cylinder assemblage model with coated fiber; (b) Equivalent composite medium.

erogeneities. "^" denotes a specific quantity in the cylindrical coordinate system. In the above equation, considering the geometry of the CNT, the displacements are assumed to depend only on the microcoordinates $(\widetilde{\theta}, \widetilde{x}_3)$ as there is no significant variation in the radial direction.

Similarly, the strains can be expressed in the following form:

$$\begin{aligned} &\widehat{\varepsilon}_{ij}^{\delta} = \widehat{\varepsilon}_{ij}^{(0)} + \delta\widehat{\varepsilon}_{ij}^{(1)} + \delta^2\widehat{\varepsilon}_{ij}^{(2)} + \cdots, \\ &\text{with } \widehat{\varepsilon}_{ij}^{(m)} = \widehat{\varepsilon}_{ij}^{(m^*)} + \frac{1}{2}\left(\widetilde{L}_i\widehat{u}_j^{(m+1)} + \widetilde{L}_j\widehat{u}_i^{(m+1)}\right), \quad m = 0, 1, 2... \end{aligned} \tag{2}$$

where

$$\begin{aligned} &\widehat{\varepsilon}_{11}^{(m^*)} = L_1\widehat{u}_1^{(m)}, \quad \widehat{\varepsilon}_{22}^{(m^*)} = L_2\widehat{u}_2^{(m)} + \frac{\widehat{u}_1^{(m)}}{r}, \quad \widehat{\varepsilon}_{33}^{(m^*)} = L_3\widehat{u}_3^{(m)}, \\ &\widehat{\varepsilon}_{23}^{(m^*)} = \frac{1}{2}\left(L_3\widehat{u}_2^{(m)} + L_2\widehat{u}_3^{(m)}\right), \quad \widehat{\varepsilon}_{13}^{(m^*)} = \frac{1}{2}\left(L_1\widehat{u}_3^{(m)} + L_3\widehat{u}_1^{(m)}\right), \\ &\widehat{\varepsilon}_{12}^{(m^*)} = \frac{1}{2}\left(L_2\widehat{u}_1^{(m)} + L_1\widehat{u}_2^{(m)} - \frac{\widehat{u}_2^{(m)}}{r}\right) \end{aligned} \tag{3}$$

where

$$\begin{aligned} &L_1 = \frac{\partial}{\partial r}, \; L_2 = \frac{1}{r}\frac{\partial}{\partial\theta}, \; L_3 = \frac{\partial}{\partial x_3}, \\ &\widetilde{L}_1 = \frac{\partial}{\partial\widetilde{r}}, \; \widetilde{L}_2 = \frac{1}{r}\frac{\partial}{\partial\widetilde{\theta}}, \; \widetilde{L}_3 = \frac{\partial}{\partial\widetilde{x}_3} \end{aligned} \tag{4}$$

Using Hooke's law $\widehat{\sigma}_{ij}^{\delta} = \widehat{C}_{ijkl}^{\delta}\widehat{\varepsilon}_{ij}^{\delta}$, and Eq. (2), the stresses can be obtained as follows:

$$\begin{aligned} &\widehat{\sigma}_{ij}^{\delta} = \widehat{\sigma}_{ij}^{(0)} + \delta\widehat{\sigma}_{ij}^{(1)} + \delta^2\widehat{\sigma}_{ij}^{(2)} + \cdots, \\ &\text{with } \widehat{\sigma}_{ij}^{(m)} = \widehat{C}_{ijkl}\widehat{\varepsilon}_{kl}^{(m^*)} + \widehat{C}_{ijkl}\widetilde{L}_k\widehat{u}_l^{(m+1)} \end{aligned} \tag{5}$$

where $\widehat{C}_{ijkl}$ denotes the position-dependent elastic stiffness which is necessarily symmetrical fourth-order tensor.

In the absence of body force, the equilibrium equations can be expressed using Eq. (5):

$$\begin{aligned} &\frac{1}{\delta}\left(\widetilde{L}_j\widehat{\sigma}_{1j}^{(0)}\right) + L_j\widehat{\sigma}_{1j}^{(0)} + \frac{\widehat{\sigma}_{11}^{(0)} - \widehat{\sigma}_{22}^{(0)}}{r} + \widetilde{L}_j\widehat{\sigma}_{1j}^{(1)} + \delta\cdots = 0 \\ &\frac{1}{\delta}\left(\widetilde{L}_j\widehat{\sigma}_{2j}^{(0)}\right) + L_j\widehat{\sigma}_{2j}^{(0)} + 2\frac{\widehat{\sigma}_{12}^{(0)}}{r} + \widetilde{L}_j\widehat{\sigma}_{2j}^{(1)} + \delta\cdots = 0 \\ &\frac{1}{\delta}\left(\widetilde{L}_j\widehat{\sigma}_{3j}^{(0)}\right) + L_j\widehat{\sigma}_{3j}^{(0)} + \frac{\widehat{\sigma}_{13}^{(0)}}{r} + \widetilde{L}_j\widehat{\sigma}_{3j}^{(1)} + \delta\cdots = 0 \end{aligned} \tag{6}$$

Following the classical asymptotic expansion homogenization, the homogenized constitutive equations of the nanocomposite interphase are defined at the order of δ^{-1}:

$$\widetilde{L}_j\widehat{\sigma}_{ij}^{(0)} = 0, \quad i = 1, 2, 3 \tag{7}$$

Using Eq. (5), Eq. (7) can be further expressed as:

$$\widetilde{L}_j\left(\widehat{C}_{ijkl}\right)\widehat{\varepsilon}_{kl}^{(0^*)} + \widetilde{L}_j\left(\widehat{C}_{ijkl}\widetilde{L}_k\widehat{u}_l^{(1)}\right) = 0 \tag{8}$$

In the above equation, $\widehat{\varepsilon}_{kl}^{(0^*)}$ depends only on the mesoscale displacements $\widehat{u}_i^{(0)}$.

Assuming that $\widehat{u}_i^{(1)} = \widehat{N}_l^{mn}\widehat{\varepsilon}_{kl}^{(0^*)}$, the solution of Eq. (8) at the order of δ^{-1} yields the homogenized properties of the nanocomposites as follows:

$$\widehat{C}_{ijmn}^{NCP} = \langle\widehat{C}_{ijmn} + \widehat{C}_{ijkl}\widetilde{L}_k\widehat{N}_l^{mn}\rangle \tag{9}$$

where $\langle\varphi\rangle = (1/A)\int_{-\widetilde{x}_3/2}^{\widetilde{x}_3/2}\int_{-\theta/2}^{\theta/2} r\varphi(r,\widetilde{\theta},\widetilde{x}_3)\mathrm{d}\widetilde{\theta}\mathrm{d}\widetilde{x}_3$ denotes the area integral symbol on the area A of the 2-D unit cell with respect to $(\widetilde{\theta}, \widetilde{x}_3)$ and $\widehat{N}_l^{mn}$ are periodic functions given by Chatzigeorgiou et al. [29].

It should be pointed out that the periodic structure of the nanocomposite interphase depends on the radial coordinate and the volume fraction decreases with increasing radial distance. The effective properties, in theory, are obtained by solving the unit cell problems multiple times, with each unit cell representing a different profile at a specific radial location. For the sake of simplicity, in this work, the nanocomposite interphase is assumed to be transversely isotropic with the axis of symmetry parallel to the axis of the CNTs. In this regard, the unit cell problem can be solved only once by considering one interfacial layer. An additional simplification employed in the present work is that the inelastic behavior of the NCP is described directly using the plastic flow rule for transversely isotropic material. Parametric investigations and applications explicitly accounting for the nonlinear deformation mechanisms of the CNTs and the surrounding matrix require a multiscale analysis methodology such as FE^2 analysis [35], which will be addressed in a forthcoming publication.

2.2. *Mesoscale: homogenization of equivalent fiber*

Having obtained the effective properties of the nanocomposite interphase, the homogenized behavior of the actual composites can be determined via either the periodic homogenization approaches such as the finite-element and finite-volume techniques, or the classical micromechanics approaches that are based on homogeneous boundary conditions. In the second step of homogenization, the CNTs and their surrounding matrix are substituted by an equivalent interphase medium which presents cylindrical orthotropy. In the Cartesian coordinates, however, the NCP exhibits spatially dependent behaviors. Under such circumstances, the finite-element and finite-volume techniques require an exceptionally refined mesh discretization in the interphase region to capture the rapidly changing interphase properties. This will ineluctably induce an increase in the computational cost. A viable alternative to the finite-element or the finite-volume-based periodic homogenization is the meshless classical micromechanics approach. Nonetheless, the latter is derived based on average stress/strain per phase and hence significantly overestimates the inelastic response.

Herein, a novel hybrid homogenization technique is developed that

makes use of the elements of the extended classical micromechanics approach based on CCA, recently developed by the present authors in Chatzigeorgiou et al. [20], and the mainstream finite-element based periodic homogenization technique. Specifically, an equivalent fuzzy fiber is created via the CCA-TFA micromechanics simulations, with the purpose of replacing the nanocomposite interphase and the main fiber, also referred to as composite fiber in this manuscript. In the third step of homogenization described in the next subsection, the composite fibers are substituted by the equivalent fibers to obtain the macroscopic stress-strain behavior of the whole fuzzy fiber composites. The current hybrid homogenization approach not only permits the accurate characterization of the inelastic deformation mechanisms in the matrix phase and the fiber-fiber interactions in multi-inclusion repeating unit cells neglected in the classical micromechanics approaches, but also avoids the three-dimensional mesh refinement in the nanocomposite coating layers if the periodic homogenization approaches are followed. The latter facilitates simulating the nanocomposite interphase of arbitrary thickness and more complex microstructures such as random fiber distributions.

The extended CCA is based on the transformation field analysis, developed by Dvorak [49], of inelastic stress fields to account for the inelastic mechanisms of each phase. Fig. 4(a) depicts a perfectly bonded multi-concentric cylinder model. The cylinder is made of three distinct phases, namely, the matrix phase (denoted by subscript 0), the interphase (denoted by subscript 2), and the inclusion (denoted by subscript 1). The inclusion occupying the space Ω_1 is represented by a constant elasticity modulus $\mathbf{L}_1$ and subjected to the inelastic stress $\boldsymbol{\sigma}_1^p$. Likewise, the matrix occupying the space Ω_0 is characterized by a constant elasticity modulus $\mathbf{L}_0$ and subjected to inelastic stress $\boldsymbol{\sigma}_0^p$. The coating layer which is subjected to the inelastic stress $\boldsymbol{\sigma}_2^p$ fills up the space Ω_2 between the matrix and the inclusion phases. The elastic modulus of the coating layer $\mathbf{L}_2(\mathbf{x})$ is, however, spatially dependent on the Cartesian coordinates due to the cylindrical orthotropic nature of the interphase material. Along the boundary of the matrix phase, a linear displacement field $\mathbf{u}^{\text{ext}} = \bar{\boldsymbol{\varepsilon}}\cdot\mathbf{x}$ is imposed, with $\bar{\boldsymbol{\varepsilon}}$ denoting the mesoscale strain tensor. The volume of each phase is represented by $V_i (i = 0, 1, 2)$. With the above definition, space $\Omega = \Omega_1 \cup \Omega_2 \cup \Omega_0$ denotes the whole representative volume element (RVE), with a volume of $V = V_1 + V_2 + V_0$.

In the absence of inertial and body forces, the governing equation of the RVE reads:

$$\text{div}\boldsymbol{\sigma} = \mathbf{0}, \text{ in } \Omega \tag{10}$$

where

$$\boldsymbol{\sigma}(\mathbf{x}) = \begin{cases} \mathbf{L}_1 : \boldsymbol{\varepsilon}(\mathbf{x}) + \boldsymbol{\sigma}_1^p & \mathbf{x} \in \Omega_1 \\ \mathbf{L}_2(\mathbf{x}) : \boldsymbol{\varepsilon}(\mathbf{x}) + \boldsymbol{\sigma}_2^p & \mathbf{x} \in \Omega_2 \\ \mathbf{L}_0 : \boldsymbol{\varepsilon}(\mathbf{x}) + \boldsymbol{\sigma}_0^p & \mathbf{x} \in \Omega_0 \end{cases} \tag{11}$$

Eq. (10) is solved based on an essential assumption that the inelastic stress per phase is uniform, which is common in the development of classical micromechanics approaches. The inelastic stresses within the composite microstructure are strongly nonuniform. This is particularly true in the matrix phase of the fuzzy fiber composites, where large stress and strain deformation gradients are expected in this phase due to the large property contrast between the composite fiber and the surrounding matrix. Like all other classical micromechanics models, the uniform inelastic stress field is a vital issue in the extended CCA-TFA approach presented herein, which produces a substantially stiff macroscopic response in generating the results that follow.

In the present analytical scheme, an equivalent medium occupying the space Ω is considered, as shown in Fig. 4(b). The macroscopic constitutive law for this equivalent medium reads:

$$\bar{\boldsymbol{\sigma}} = \bar{\mathbf{L}} : \bar{\boldsymbol{\varepsilon}} + \bar{\boldsymbol{\sigma}}^p \tag{12}$$

where $\bar{\mathbf{L}}$ is the unknown effective elasticity tensor and $\bar{\boldsymbol{\sigma}}^p$ is the effective inelastic stress tensor. $\bar{\boldsymbol{\sigma}} = \sum_{i=0}^{2} c_i\boldsymbol{\sigma}_i$ and $\bar{\boldsymbol{\varepsilon}} = \sum_{i=0}^{2} c_i\boldsymbol{\varepsilon}_i$, with $c_i = V_i/V$ denoting the volume fraction of each phase.

Following the TFA method, the averaged strain per phase is expressed as a function of the applied macroscopic strain and the inelastic stresses from all phases as [20]:

$$\boldsymbol{\varepsilon}_i = \mathbf{A}_i : \bar{\boldsymbol{\varepsilon}} + \sum_{j=0}^{2} \mathbf{A}_{j,i}^p : \boldsymbol{\sigma}_j^p \tag{13}$$

where $\mathbf{A}_i$ and $\mathbf{A}_{j,i}^p$ are the strain-type elastic and inelastic concentration tensors. $\boldsymbol{\sigma}_j^p$ is assumed to be a constant per phase. Similarly, the average stress per phase may be expressed as [20]:

$$\boldsymbol{\sigma}_i = \mathbf{D}_i : \bar{\boldsymbol{\varepsilon}} + \sum_{j=0}^{2} \mathbf{D}_{j,i}^p : \boldsymbol{\sigma}_j^p \tag{14}$$

where $\mathbf{D}_i$ and $\mathbf{D}_{j,i}^p$ are the stress-type elastic and inelastic concentration tensors.

Combining Eqs. (12) and (14) yields:

$$\bar{\mathbf{L}} = \sum_{i=0}^{2} c_i\mathbf{D}_i, \quad \bar{\boldsymbol{\sigma}}^p = \sum_{j=0}^{2} \mathbf{B}_j^p : \bar{\boldsymbol{\sigma}}_j, \quad \mathbf{B}_j^p = \sum_{i=0}^{2} c_i\mathbf{D}_{j,i}^p \tag{15}$$

Following the classical composite cylinder assemblage approach, several boundary value problems are solved analytically under axisymmetric and anti-plane shear loading conditions to identify the elastic and inelastic concentration tensors. For the transverse shear loading, the generalized self-consistent composite cylinder assemblage model is adopted. The readers are referred to our recent work, Chatzigeorgiou et al. [20], for a detailed derivation of these tensors.

In this contribution, to address the overestimation of the inelastic stress-strain behavior of fuzzy fiber composites in the case of CCA-TFA being followed, an equivalent fiber is obtained when the volume of the matrix approaches zero. This equivalent fiber is subsequently integrated into the macroscale homogenization elaborated in the following subsection to mimic the inelastic response of the composite fiber.

2.3. *Macroscale: hybrid homogenization of equivalent fiber embedded in a matrix*

In the third step of homogenization, the macroscopic constitutive relation of the whole fuzzy fiber composites is obtained. The macroscale repeating unit cell is considered to possess two unique phases, i.e., the equivalent fiber and the surrounding matrix. The matrix phase is assumed to be elastic-plastic material which is described by classical J_2 elastoplasticity. The equivalent fiber is elastic-plastic, the response of which is given by the lower-scale CCA-TFA analysis. Under these conditions, homogenization of the second periodic boundary value problems can be achieved using the standard asymptotic expansion homogenization at the order of δ^{-1}, interpreted in the Cartesian coordinate system, cf. Chatzigeorgiou et al. [50].

3. Verification and assessment

In this section, the inelastic behavior of a fuzzy fiber composite is generated under various loading conditions to assess the accuracy of the proposed hybrid homogenization vis-à-vis the classical CCA-TFA, as well as the classical periodic homogenization approach.

The fuzzy fiber composites investigated herein consist of three material phases. The matrix is assumed to be epoxy, which is represented by the classical elastoplasticity of isotropic material. The main fiber is made of isotropic glass which is taken to be elastic during the entire deformation history. The carbon nanotube is made of graphene which is also isotropic. The elastic properties for all these materials taken from

Table 1
Elastic properties of the fuzzy fiber composite constituents (Chatzigeorgiou et al. [22]).

	E (GPa)	ν
Epoxy	3	0.3
Glass	72	0.2
Graphene	1100	0.14

Table 2
Effective properties of the nanocomposite obtained via periodic homogenization.

Properties	$\bar{k}$	$\bar{l}$	$\bar{n}$	$\bar{\mu}^{tr}$	$\bar{\mu}^{ax}$
Value (MPa)	5758.1	2526	299714	2523.6	2807.1

Chatzigeorgiou et al. [22] are listed in Table 1. At the microscopic scale, the internal and external radii of the CNTs are $0.51nm$ and $0.85nm$, respectively, cf. Chatzigeorgiou et al. [22]. At the mesoscale, the glass fiber radius is equal to $2.5\mu m$, and the length of the CNTs is taken to be $2\mu m$. The volume fraction of the composite fiber (NCP + main fiber) over the whole fuzzy fiber composite system is 30%.

For the sake of simplicity, the nanocomposite interphase is considered to be transversely isotropic with the axis of symmetry parallel to the axis of the CNTs. The elastic tensor of the equivalent nanocomposite interphase reads:

$$\overline{\mathbf{L}}_2 = \begin{bmatrix} \bar{k}+\bar{\mu} & \bar{k}-\bar{\mu} & \bar{l} & 0 & 0 & 0 \\ \bar{k}-\bar{\mu} & \bar{k}-\bar{\mu} & \bar{l} & 0 & 0 & 0 \\ \bar{l} & \bar{l} & \bar{n} & 0 & 0 & 0 \\ 0 & 0 & 0 & \bar{\mu}^{tr} & 0 & 0 \\ 0 & 0 & 0 & 0 & \bar{\mu}^{ax} & 0 \\ 0 & 0 & 0 & 0 & 0 & \bar{\mu}^{ax} \end{bmatrix} \tag{16}$$

In the above equation, $\bar{k}$ denotes the plane strain bulk modulus, $\bar{\mu}^{tr}$ denotes the transverse shear modulus, $\bar{\mu}^{ax}$ denotes the axial shear modulus, $\bar{n}$ is the modulus related to the axial tensile loading, and $\bar{l}$ reflects the coupling between the axial tension and transverse tension loadings. It should be pointed out that the scope is to investigate the accuracy of the proposed methodology for capturing the inelastic mechanisms at the mesoscopic hence macroscopic scale. In order not to deviate from this goal, the NCP is treated as a homogeneous medium whose inelastic behavior is described directly using the plastic flow rule for transversely isotropic material, Long et al. [51]. Parametric investigations and applications involving nonlinear analysis of CNTs and surrounding matrix will be addressed in a forthcoming publication.

At the microscale analysis, the periodic boundary conditions are imposed at the boundary of the repeating unit cell. To establish the complete elastic stiffness tensor, the unit cell problems are solved six times by applying sequentially one nonzero unit mesoscopic strain at a time, Chatzigeorgiou et al. [20]. Herein, the equivalent properties of the nanocomposite interphase obtained via the finite-element package ABAQUS are listed in Table 2 and they are directly utilized in the second step of the mesoscale analysis.

Concerning the plastic parameters, the yield surface of the elastoplastic matrix reads:

$$\Phi = \sigma^{VM} - Y - Q[1-\exp(-bp)] \tag{17}$$

where σ^{VM} and p are the Von Mises equivalent stress and the cumulative effective plastic strain, respectively. Ydenotes the initial yield strength and Q indicates the difference between the saturation and initial yielding stresses. b represents the hardening rate.

In the case of NCP, the transversely isotropic elastoplasticity theory is employed. As such, the yield surface may be decomposed into in-plane and axial shear loadings:

Table 3
Plastic properties of the matrix and the NCP.

Matrix		NCP	
Y(MPa)	20	Y_t (MPa)	30
Q (MPa)	30	Q_t (MPa)	160
b	200	b_t	3
		Y_a (MPa)	30
		Q_a (MPa)	160
		b_a	3

$$\begin{aligned} \Phi_t &= \sqrt{\tfrac{1}{2}s_{ij}^t s_{ij}^t} - Y_t - Q_t[1-\exp(-b_t p_t)], \\ \Phi_a &= \sqrt{\frac{1}{2}s_{ij}^a s_{ij}^a} - Y_a - Q_a[1-\exp(-b_a p_a)] \end{aligned} \tag{18}$$

where the subscripts (or superscripts) t and a indicate inplane and axial shear loading respectively. For a transversely isotropic elastoplastic material with the axis of symmetry parallel to direction 3,

$$\begin{aligned} s_{ij}^t &= \sigma_{ij} + \sigma_{33}\delta_{i3}\delta_{j3} - \widetilde{\sigma}\left[\delta_{ij} - \delta_{i3}\delta_{j3}\right] - \left[\sigma_{i3}\delta_{j3} + \sigma_{j3}\delta_{i3}\right], \\ s_{ij}^a &= \left[\sigma_{i3}\delta_{j3} + \sigma_{j3}\delta_{i3}\right] - 2\sigma_{33}\delta_{i3}\delta_{j3} \end{aligned} \tag{19}$$

where $\widetilde{\sigma} = (\sigma_{11} + \sigma_{22})/2$. In the present work, the plastic properties listed in Table 3 will be used in generating results that follow.

The homogenized nonlinear stress-strain behaviors of the fuzzy fiber composites are obtained following three different approaches: (1) via the hybrid homogenization method (HHM) with two distinct phases (the equivalent fiber and matrix) proposed in the present work; (2) via the classical full-field homogenization (FFH) with three distinct phases (the main fiber, NCP, and matrix); (3) via the recently developed CCA-TFA theory, cf., Chatzigeorgiou et al. [20]. The full-field homogenization is considered to be the most accurate hence it is used as a gold standard to assess the accuracy of both the HHM and CCA-TFA approaches.

Fig. 5(a) and (b) show the repeating unit cells used in FFH and HHM calculations, which are discretized into 12096 and 12548 fully integrated ten-node tetrahedral elements, respectively. For both cases, the composite fibers are distributed in the matrix phase periodically in a square arrangement. Exactly the same mesh discretization in the matrix was adopted in both FFH and HHM simulations, while the total number of elements in the equivalent fiber and the fiber/interphase domain has been kept as closely as possible. Finer meshes have also been used to validate the generated results based on the chosen mesh discretizations but do not yield any differences, indicating converged unit cell solutions based on the present mesh discretizations. This mesh refinement is not presented in this paper to keep it concise. It is worth noting that while the NCP is transversely isotropic in the cylindrical coordinates, it presents spatially-dependent monoclinic mechanical behavior in the Cartesian coordinates. Due to this spatial dependency, greater mesh discretizations in the affected region are required to capture the rapid variation of interphase properties. The field quantities within the nanocomposite domain also change more drastically. Smaller step size (hence more loading increments) is (are) preferred in the classical full-field homogenization simulation which is necessary to ensure numerical stabilities.

Fig. 6 presents the comparison of the homogenized stress-strain response of the fuzzy fiber composites generated by the HHM, FFH, and CCA-TFA approaches. Uniaxial strain-controlled loading and stress-controlled unloading tests are performed under transverse tensile, longitudinal tensile, transverse shear, axial shear loading paths. It is evident that the FFH and HHM results show a good level of accordance during the entire loading-unloading history under every loading condition. In contrast, the classical micromechanics approach based on CCA-TFA can only provide reasonable estimations of the stress-strain curves under the longitudinal tensile loading path. It predicts significantly stiffer stress-

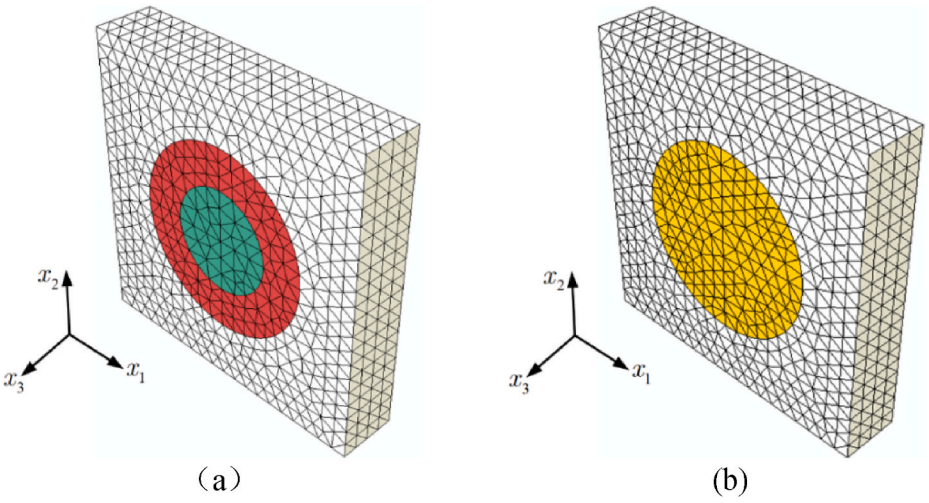

Fig. 5. (a) Repeating unit cell containing fiber, nanocomposite interphase, and matrix phases; (b) Repeating unit cell containing equivalent fiber and matrix phases.

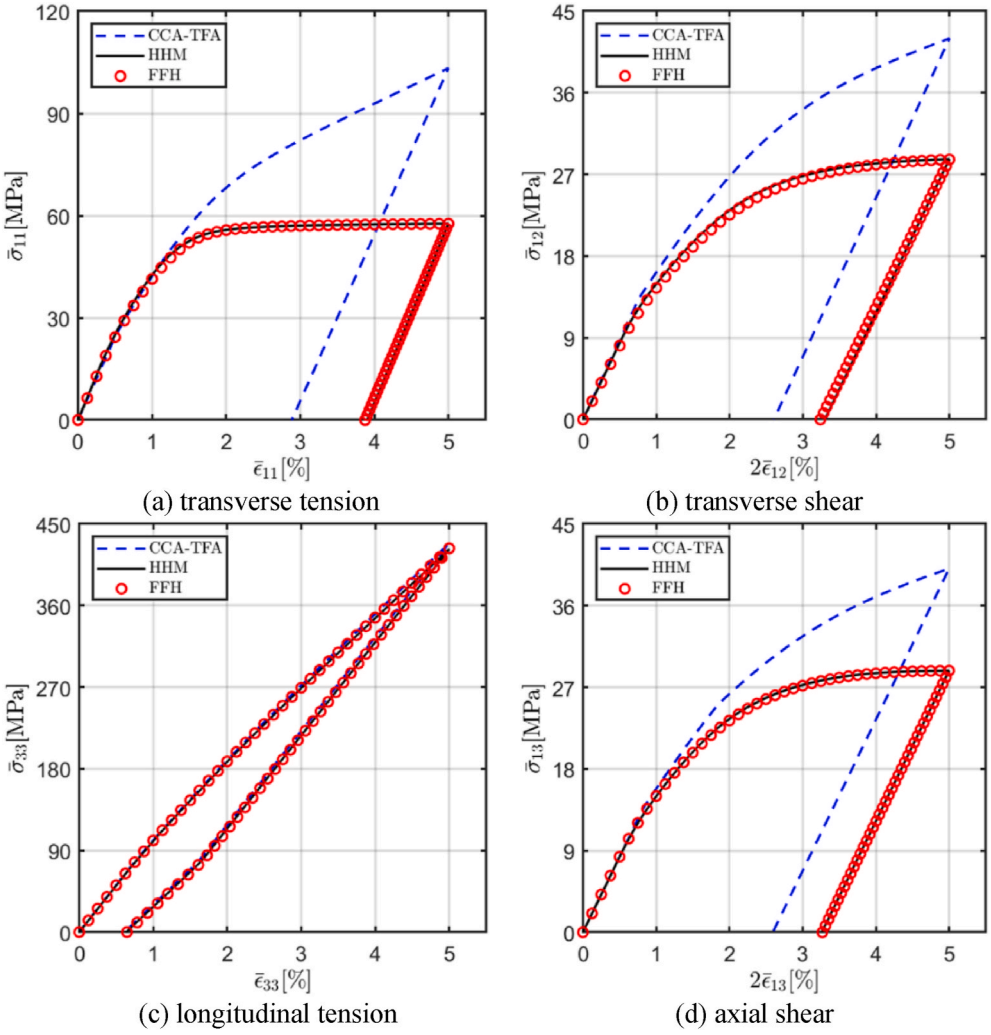

Fig. 6. Comparison of the uniaxial homogenized response of the fuzzy fiber composites based on FFH, HHM, and CCA-TFA approaches.

strain behavior under transverse tensile, transverse shear, and axial shear loading cases, relative to the FFH and HHM approaches. The main reason for this discrepancy, frequently observed between the mean-field and full-field approaches, is that the CCA-TFA neglects the fiber-fiber interactions, which leads to the stress field inside the composites cannot be properly captured. In addition to the fiber-fiber interactions, the CCA-TFA is developed based on averaged inelastic stress per phase, thus it cannot capture the plastic strain localization inside the plastic phase. When the plastic strains are significant, the plastic flow changes drastically in terms of evolution that affects the concomitant

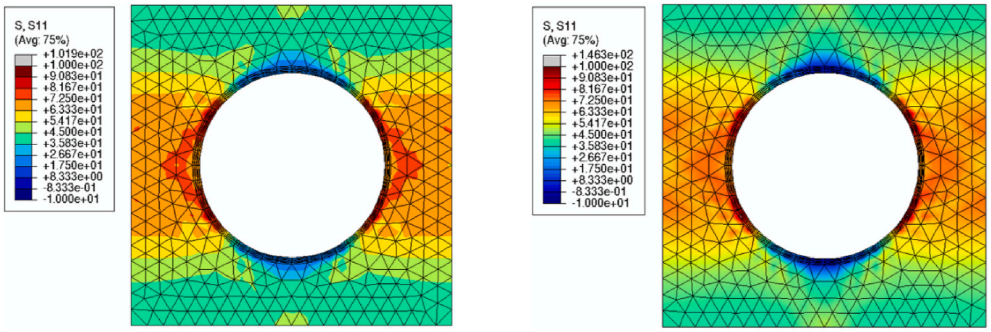

Fig. 7. Comparison of matrix transverse normal stress σ_{11} distributions at the macroscopic strain of $\overline{\varepsilon}_{11} = 2.5\%$ under uniaxial loading by $\overline{\sigma}_{11} \neq 0$ obtained using FFH and HHM approaches.

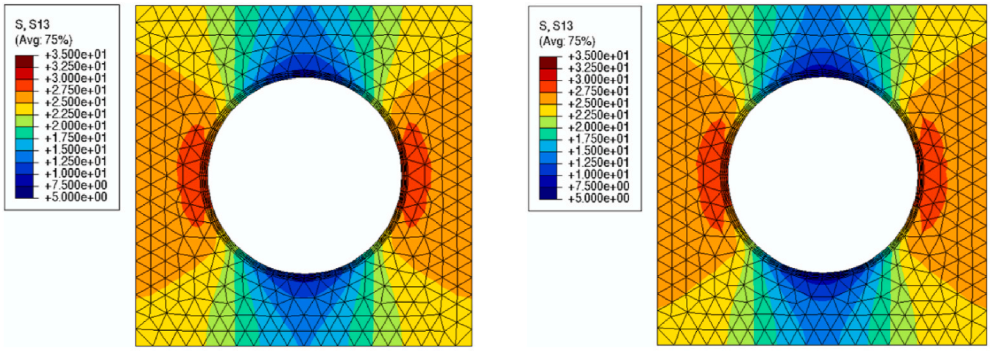

Fig. 8. Comparison of matrix axial shear stress σ_{13} distributions at the macroscopic strain of $2\overline{\varepsilon}_{13} = 2.5\%$ under uniaxial loading by $\overline{\sigma}_{13} \neq 0$ obtained using FFH and HHM approaches.

macroscopic stresses. The ability to capture the spatially varying inelastic stress field is more essential in the case of fuzzy fiber composites due to the large property contrast between the constituent materials observed in this type of material.

The importance of accurate prediction of local stress fields on the design of durable composite materials, herein the fuzzy fiber composites, cannot be overstated [52]. To assess the capability of the HHM in predicting the stress localizations induced by the microstructures, in the following, the stress fields predicted by the HHM are extensively verified vis-à-vis the FFH results which are the gold standard. Fig. 7 presents the differences between the matrix transverse normal stress σ_{11}distributions generated by the FFH and HHM approaches, at the macroscopic strain level of $\overline{\varepsilon}_{11} = 2.5\%$ under the uniaxial loading $\overline{\sigma}_{11}$ branch. Fig. 8 presents the differences between the matrix axial shear stress σ_{13} distributions generated by the FFH and HHM approaches, at the macroscopic strain level of $2\overline{\varepsilon}_{13} = 2.5\%$ under the uniaxial shear loading $\overline{\sigma}_{13}$ branch. As observed, the HHM produces nearly identical stress distributions noted in the FFH predictions almost everywhere for both transverse tensile and axial shear loadings, even in the vicinity of the composite fiber where significant plastic field localizations are expected. This suggests that the HHM can properly capture the local inelastic deformation mechanisms in the matrix phase neglected in the classical mean-field homogenization theories and hence the concomitant macroscopic response. The advantage of HHM over the classical full-field homogenization lies in the elimination of interphase mesh discretization, which may be exceptionally exhausting for periodic fuzzy fiber arrays with complex or random fiber microstructures. Another significance of the hybrid approach is that it enables simulating fuzzy fiber composites of arbitrary thickness that may be used in parametric studies for understanding the microstructure-property relationship over large parameter space.

Table 4
Comparison of average phase stress σ_{11} (MPa) as a function of applied loading $\overline{\varepsilon}_{11}$ (%) generated by CCA-TFA, HHM, and FFM under uniaxial transverse tension by.$\overline{\sigma}_{11} \neq 0$

Materials	$\overline{\varepsilon}_{11}$ (%)	1.25	2.5	3.75	5
Equivalent Fiber /NCP + Fiber	CCA-TFA	67.08	110.32	141.77	172.00
	HHM	63.22	69.40	68.02	66.87
	FFH	61.57	69.28	67.88	66.70
Matrix	CCA-TFA	42.74	61.33	68.14	73.82
	HHM	42.30	51.24	52.78	53.69
	FFH	41.69	51.20	52.80	53.74

Table 5
Comparison of average phase stress σ_{13} (MPa) as a function of applied loading $2\overline{\varepsilon}_{13}$ (%) generated by CCA-TFA, HHM, and FFM under uniaxial axial shear loading by.$\overline{\sigma}_{13} \neq 0$

Materials	$2\overline{\varepsilon}_{13}$ (%)	1.25	2.5	3.75	5
Equivalent Fiber /NCP + Fiber	CCA-TFA	26.57	44.25	56.26	66.88
	HHM	23.26	33.20	34.98	35.14
	FFH	23.29	32.75	34.68	34.88
Matrix	CCA-TFA	15.33	23.46	27.38	28.57
	HHM	15.11	22.66	25.54	26.13
	FFH	15.11	22.66	25.63	26.24

Quantitative comparisons of the average stresses per phase predicted by three approaches at different levels of macroscopic strain are summarized in Tables 4 and 5 for the transverse tensile and the axial shear loadings, respectively. It should be noted that in the case of HHM

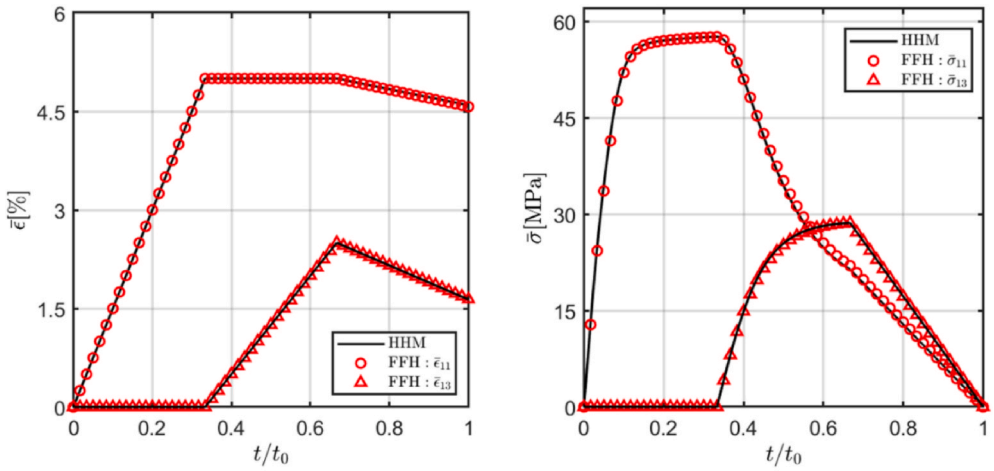

(a) Strain V.S. time (b) Stress V.S. time

Fig. 9. Comparison of the homogenized response of the fuzzy fiber composites based on FFH and HHM under the biaxial transverse tension-axial shear loading path.

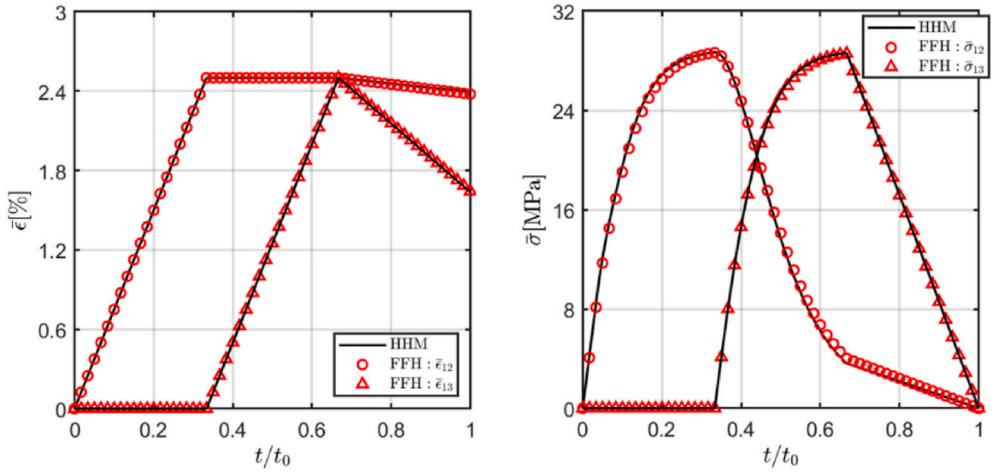

(a) Strain V.S. time (b) Stress V.S. time

Fig. 10. Comparison of the homogenized response of the fuzzy fiber composites based on FFH and HHM under the biaxial transverse shear-axial shear loading path.

prediction, the average stresses over the equivalent fiber are evaluated, which correspond to the average stresses over the main fiber and NCP in the case of FFH and CCA-TFA simulations. Again, it is observed that while the correlations of the average phase stresses between the HHM and FFH approaches are remarkable at every loading step, the CCA-TFA predicts exceedingly higher stresses in the plastic loading range, and perhaps even the stresses in the elastic stage. The second observation is that increasing the macroscopic strain accentuates the differences between the CCA-TFA and the HHM/FFH results caused by the continuing microstructure-induced plastic field localization neglected in the classical CCA-TFA approach.

4. Numerical results

4.1. Single inclusion case

Thus far, there has been no reported data in the open literature on the macroscopic inelastic response of periodic fuzzy fiber arrays under arbitrary multiaxial loading paths. Such knowledge is important to efficiently design durable and sustainable structural components made of fuzzy fiber composites to meet the specific needs of applications. In this subsection, the biaxial and triaxial loading numerical experiments were conducted to demonstrate the hybrid homogenization approach's ability to analyze periodic fuzzy fiber arrays subjected to more complex nonproportional loading conditions. As demonstrated in the previous subsection, the classical CCA-TFA approach fails to capture the inelastic deformations under uniaxial transverse tension, transverse shear, and axial shear loading cases. Hence the numerical examples presented herein provide a very demanding test of the new method's accuracy.

Fig. 9 illustrates the comparison of the biaxial homogenized stress-strain response generated by the hybrid homogenization method vis-à-vis the classical full-field homogenization. At the first stage, the fuzzy fiber composite is subjected to strain-controlled uniaxial stress loading by $\bar{\sigma}_{11} \neq 0$ up to $\bar{\varepsilon}_{11} = 5\%$. At the second stage, linearly increasing axial shear strain $\bar{\varepsilon}_{13}$ is imposed till $\bar{\varepsilon}_{13} = 2.5\%$ while the $\bar{\varepsilon}_{11}$ has been kept the same. The third stage is stress-controlled unloading. An excellent agreement between the HHM and FFH results is observed, suggesting the hybrid approach's capability to capture the inelastic deformation mechanisms under multiaxial loading conditions. Comparison of the homogenized stress-strain response generated by the FFH and HHM under the biaxial transverse shear and axial shear loading paths is presented in Fig. 10. Similar to the previous case, the fuzzy fiber composite is first subjected to strain-controlled transverse shear loading by $\bar{\sigma}_{12} \neq 0$ up to $\bar{\varepsilon}_{12} = 2.5\%$. Then, linearly increasing axial shear strain $\bar{\varepsilon}_{13}$ is

imposed till $\bar{\varepsilon}_{13} = 2.5\%$ while the $\bar{\varepsilon}_{12}$ has been kept the same, which is followed by stress-controlled unloading. Once again, no visible differences are observed between the FFH and HHM predictions.

Fig. 11 presents the comparison of the homogenized stress-strain response of fuzzy fiber composites under triaxially loaded in-plane tension-axial shear paths obtained by the two approaches. In this case, the fuzzy fiber composite is loaded by equal biaxial tension by $\bar{\varepsilon}_{11} = \bar{\varepsilon}_{22} = \varepsilon^0$ till $\varepsilon^0 = 5\%$. Next, linearly increasing axial shear strain $\bar{\varepsilon}_{13}$ is superposed till $\bar{\varepsilon}_{13} = 2.5\%$. The third stage is still stress-controlled unloading. It is evident that the HHM coincides with FFH during the entire loading history. Fig. 12 illustrates the comparison of the macroscopic response of fuzzy fiber composites under triaxially loaded in-plane tension-transverse shear paths by the FFH and HHM approaches. The fuzzy fiber composite is loaded by biaxial tension by $\bar{\varepsilon}_{11} = 2\bar{\varepsilon}_{22} = \varepsilon^0$ till $\varepsilon^0 = 5\%$. In the second loading stage, linearly increasing transverse shear strain $\bar{\varepsilon}_{12}$ is superposed till $\bar{\varepsilon}_{12} = 2.5\%$. As customary, the third stage is stress-controlled unloading. It is remarkable how well the HHM is capable of capturing the inelastic deformation predicted by the reference FFH results, further lending credence to the new hybrid approach's rigorous validation.

4.2. *Multi-inclusion case*

In the last subsection, the hybrid homogenization technique is employed to investigate the homogenized and local inelastic response of fuzzy fiber composites with more complex microstructures by increasing the number of inclusions to 3, Fig. 13. The ability to simulate irregular multi-inclusion periodic microstructure is a substantial advantage of the HHM over the classical or extended mean-field approaches. Hence the cases considered in this section highlight the new hybrid theory's special strengths and predictive capabilities.

The repeating unit cells were produced by placing a fiber in the center of the left-hand side half-plane and two fibers uniformly in the right-hand side subdomain. The characteristic size of the main fiber and the nanocomposite interphase remains unaffected, while the length and width of the unit cell are twice the sizes of the previous case, yielding a periodic array with a total volume fraction of 22.5%. As well-documented in the literature, the importance of the fiber-fiber interaction in such configuration cannot be overstated in terms of plastic field evolution and localization, the neglect of which is typically considered to be the main reason for the overestimation of post-yielding stress-strain response in numerical simulations. Fig. 14 depicts the homogenized loading/unloading stress-strain response for the fuzzy fiber

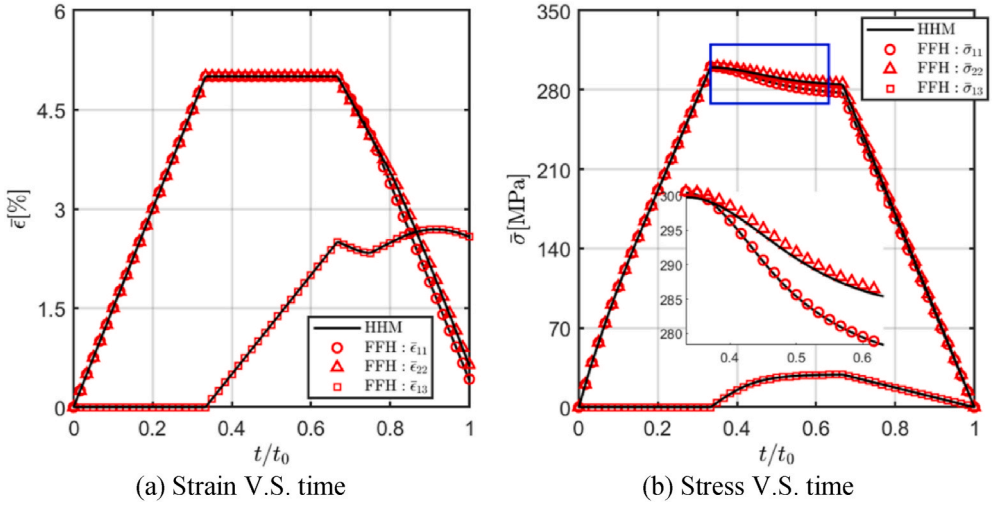

(a) Strain V.S. time (b) Stress V.S. time

Fig. 11. Comparison of the homogenized response of the fuzzy fiber composites based on FFH and HHM under the triaxial transverse tension-axial shear loading path.

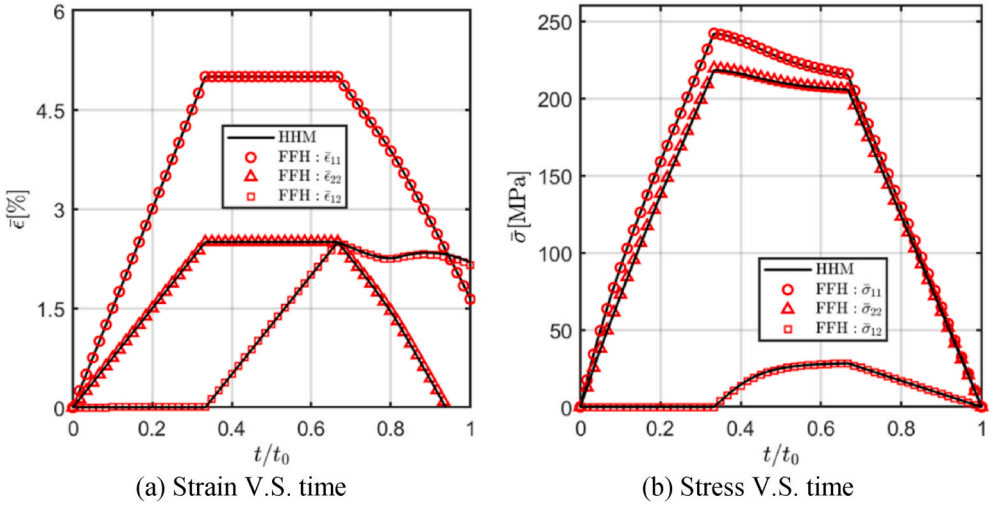

(a) Strain V.S. time (b) Stress V.S. time

Fig. 12. Comparison of the homogenized response of the fuzzy fiber composites based on FFH and HHM under the triaxial transverse tension-transverse shear loading path.

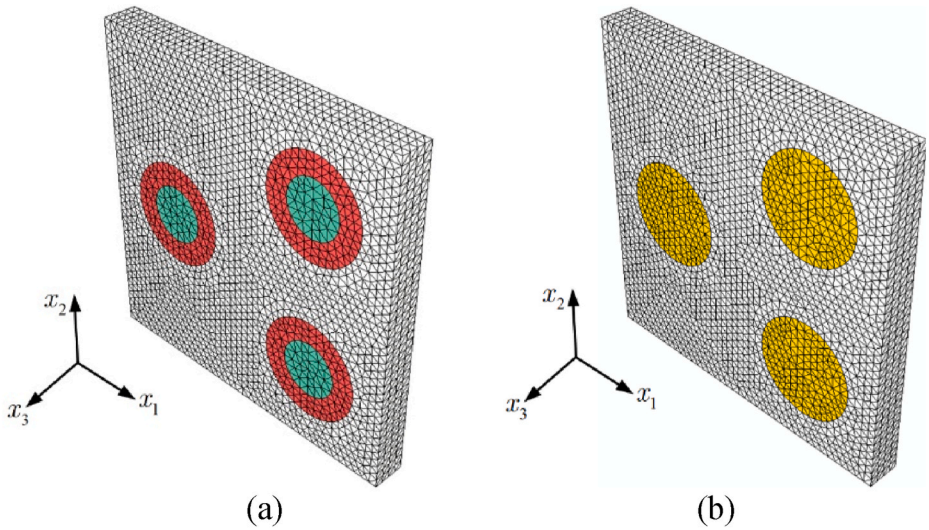

Fig. 13. (a) Multi-inclusion repeating unit cell containing three coated fibers (b) Multi-inclusion repeating unit cell containing three equivalent fibers.

composites with the muti-inclusion periodic arrangement shown in Fig. 13. The numerical experiments were conducted for uniaxial transverse tensile, transverse shear, and axial shear loadings. The previous results clearly indicate that the classical CCA-TFA approach exhibits a large deviation from the full-field reference solutions under such loading conditions, hence they are excellent candidates to test the accuracy of the new hybrid approach. As anticipated, the differences between the FFH and HHM results are really negligible during the whole loading/unloading history. Fig. 15 shows the local stress σ_{11} fields at the macroscopic strain of 2.5% during the uniaxial transverse tensile

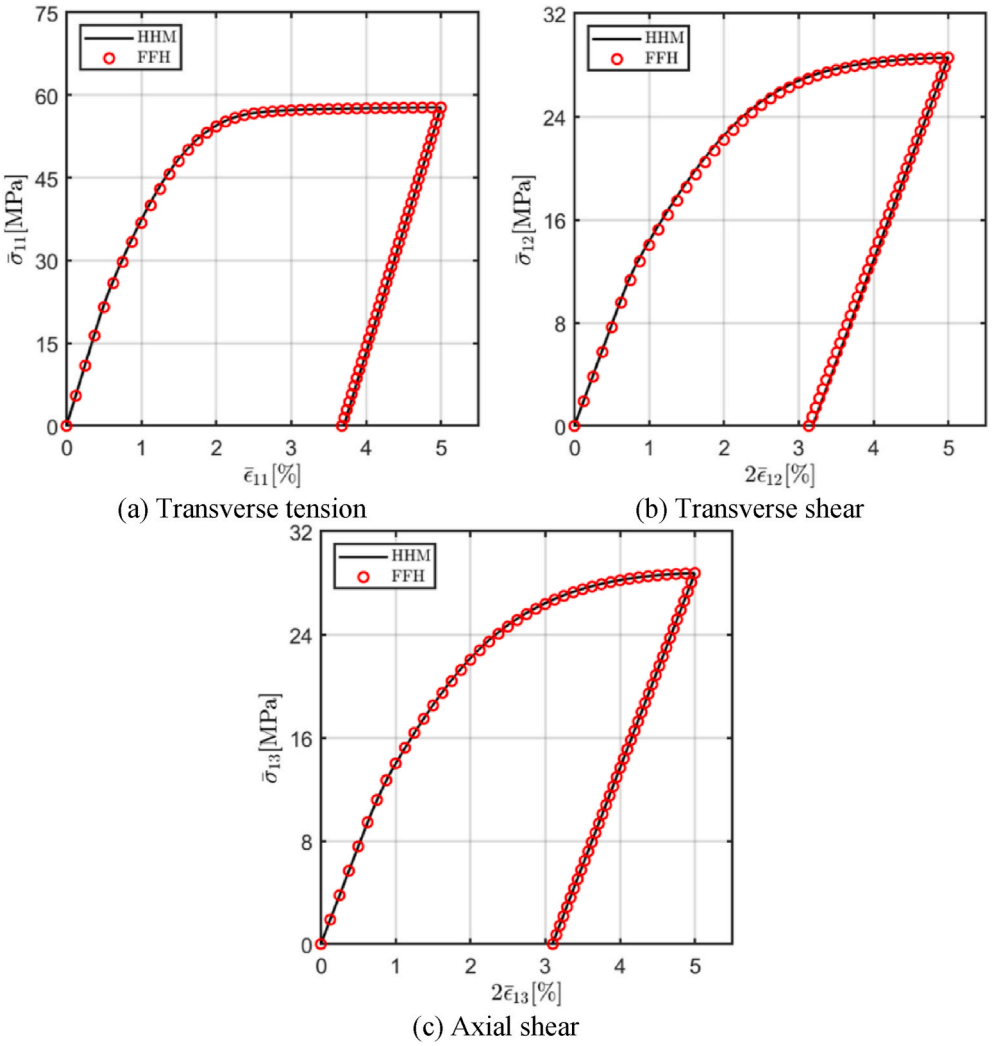

Fig. 14. Comparison of load/unload stress-strain response of multi-inclusion repeating unit cell generated by FFH with coated fibers and HHM with equivalent fibers.

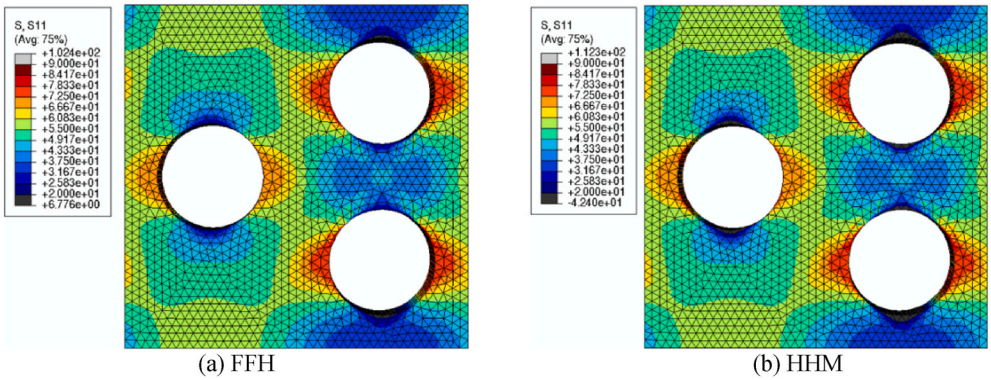

Fig. 15. Comparison of matrix stress σ_{11} distributions of multi-inclusion repeating unit cell generated by FFH with coated fibers and HHM with equivalent fibers at the applied macroscopic strains of $\bar{\varepsilon}_{11} = 2.5\%$

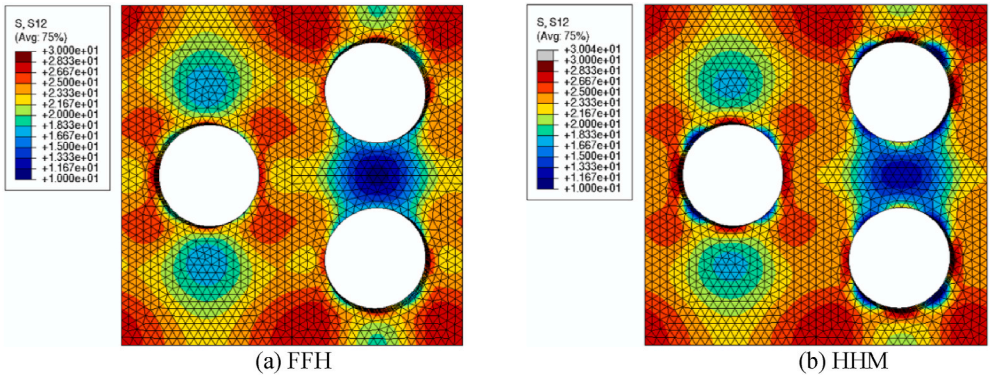

Fig. 16. Comparison of matrix stress σ_{12} distributions of multi-inclusion repeating unit cell generated by FFH with coated fibers and HHM with equivalent fibers at the applied macroscopic strains of $2\bar{\varepsilon}_{12} = 2.5\%$

loading, generated by the FFH and HHM methods, for which excellent agreement is obtained. The results immediately demonstrate the interactions between the three fibers, producing drastically changing local stress fields in the matrix phase, hence the plastic flow and plastic field localization. Comparison of the transverse shear stress σ_{12} profiles generated by the FFH and HHM approaches is presented in Fig. 16, where a macroscopic strain of $2\bar{\varepsilon}_{12} = 2.5\%$ is applied. Similar comments in terms of microstructure-induced stress fields can be applied for this loading condition.

5. Summary and conclusions

The present paper introduces a novel hierarchical homogenization theory for predicting the thus-far little-explored inelastic response of fuzzy fiber composites. This new theory combines the elements of the previously developed classical CCA-TFA, as well as the AEH homogenization theories for periodic fuzzy fiber composites accounting for inelastic mechanisms. Specifically, an equivalent fiber is created by the classical CCA-TFA analysis, which is utilized to substitute the nanocomposite interphase and the main fiber in the full-field homogenization. The significance of the new hybrid homogenization approach is the elimination of the tedious interphase mesh discretizations and the related refinement in the classical full-field homogenization along with capturing the fiber-fiber interaction neglected in the classical CCA-TFA approach.

Results generated from the new approach are compared extensively with the classical CCA-TFA and the full-filed analysis for single and multi-inclusion periodic fuzzy fiber arrays under various loading conditions. It is demonstrated that the classical CCA-TFA approach significantly overshoots the post-yielding stress-strain response for transverse tensile, transverse shear, and axial shear loadings. In contrast, the hybrid homogenization technique is capable of accurately capturing the homogenized inelastic stress-strain response of fuzzy fiber composites obtained by the reference classical full-field homogenization. The present work provides a path towards efficiently identifying the inelastic response of fuzzy fiber composites in parametric studies for design nanocomposite interphase with improved performance, an area that deserves attention and requires further investigation due to the limited knowledge.

CRediT authorship contribution statement

Qiang Chen: Writing – original draft, Formal analysis, Investigation, Validation. **George Chatzigeorgiou:** Writing – review & editing, Conceptualization, Methodology, Investigation. **Fodil Meraghni:** Conceptualization, Methodology, Writing – review & editing, Project administration.

Declaration of competing interest

The authors declare that they have no known competing financial interests or personal relationships that could have appeared to influence the work reported in this paper.

References

[1] Q. Song, K.-z. Li, H.-l. Li, H.-j. Li, C. Ren, Grafting straight carbon nanotubes radially onto carbon fibers and their effect on the mechanical properties of carbon/carbon composites, Carbon 50 (2012) 3949–3952.
[2] M.K. Hassanzadeh-Aghdam, R. Ansari, A. Darvizeh, Micromechanical analysis of carbon nanotube-coated fiber-reinforced hybrid composites, Int. J. Eng. Sci. 130 (2018) 215–229.

[3] H. Qian, E.S. Greenhalgh, M.S. Shaffer, A. Bismarck, Carbon nanotube-based hierarchical composites: a review, J. Mater. Chem. 20 (2010) 4751–4762.
[4] J. Karger-Kocsis, H. Mahmood, A. Pegoretti, All-carbon multi-scale and hierarchical fibers and related structural composites: a review, Compos. Sci. Technol. 186 (2020) 107932.
[5] M.A. Aravand, O. Shishkina, I. Straumit, A.H. Liotta, S.S. Wicks, B.L. Wardle, S. V. Lomov, L. Gorbatikh, Internal geometry of woven composite laminates with "fuzzy" carbon nanotube grafted fibers, Compos. Appl. Sci. Manuf. 88 (2016) 295–304.
[6] V.N. Popov, Carbon nanotubes: properties and application, Mater. Sci. Eng. R Rep. 43 (2004) 61–102.
[7] F.T. Fisher, R.D. Bradshaw, L.C. Brinson, Fiber waviness in nanotube-reinforced polymer composites—I: modulus predictions using effective nanotube properties, Compos. Sci. Technol. 63 (2003) 1689–1703.
[8] P.-C. Ma, N.A. Siddiqui, G. Marom, J.-K. Kim, Dispersion and functionalization of carbon nanotubes for polymer-based nanocomposites: a review, Compos. Appl. Sci. Manuf. 41 (2010) 1345–1367.
[9] D.B. Anthony, H. Qian, A.J. Clancy, E.S. Greenhalgh, A. Bismarck, M.S.P. Shaffer, Applying a potential difference to minimise damage to carbon fibres during carbon nanotube grafting by chemical vapour deposition, Nanotechnology 28 (2017) 305602.
[10] Q. Li, J.S. Church, M. Naebe, B.L. Fox, A systematic investigation into a novel method for preparing carbon fibre–carbon nanotube hybrid structures, Compos. Appl. Sci. Manuf. 90 (2016) 174–185.
[11] R. Li, N. Lachman, P. Florin, H.D. Wagner, B.L. Wardle, Hierarchical carbon nanotube carbon fiber unidirectional composites with preserved tensile and interfacial properties, Compos. Sci. Technol. 117 (2015) 139–145.
[12] S. Aziz, S.A. Rashid, S. Rahmanian, M.A. Salleh, Experimental evaluation of the interfacial properties of carbon nanotube coated carbon fiber reinforced hybrid composites, Polym. Compos. 36 (2015) 1941–1950.
[13] J. Qin, C. Wang, Z. Yao, Z. Ma, Q. Gao, Y. Wang, Q. Wang, H. Wei, Growing carbon nanotubes on continuous carbon fibers to produce composites with improved interfacial properties: a step towards commercial production and application, Compos. Sci. Technol. 211 (2021) 108870.
[14] Z. Xia, L. Riester, W.A. Curtin, H. Li, B.W. Sheldon, J. Liang, B. Chang, J.M. Xu, Direct observation of toughening mechanisms in carbon nanotube ceramic matrix composites, Acta Mater. 52 (2004) 931–944.
[15] J.J. Telega, A. Gałka, S. Tokarzewski, Application of the reiterated homogenization to determination of effective noduli of a compact bone, J. Theor. Appl. Mech. 37 (1999) 687–706.
[16] M. Barral, G. Chatzigeorgiou, F. Meraghni, R. Léon, Homogenization using modified Mori-Tanaka and TFA framework for elastoplastic-viscoelastic-viscoplastic composites: theory and numerical validation, Int. J. Plast. 127 (2020) 102632.
[17] Q. Chen, G. Chatzigeorgiou, F. Meraghni, Extended mean-field homogenization of viscoelastic-viscoplastic polymer composites undergoing hybrid progressive degradation induced by interface debonding and matrix ductile damage, Int. J. Solid Struct. 210–211 (2021) 1–17.
[18] Y. Cheng, K. Zhang, B. Liang, H. Cheng, G. Hou, G. Xu, W. Jin, Micromechanics of CNT grafted FRP based on hierarchical homogenization of transversely isotropic multi-coated model, Int. J. Mech. Sci. 161–162 (2019) 105014.
[19] S. Kundalwal, M. Ray, Micromechanical analysis of fuzzy fiber reinforced composites, Int. J. Mech. Mater. Des. 7 (2011) 149–166.
[20] G. Chatzigeorgiou, F. Meraghni, N. Charalambakis, A. Benaarbia, Multiscale modeling accounting for inelastic mechanisms of fuzzy fiber composites with straight or wavy carbon nanotubes, Int. J. Solid Struct. 202 (2020) 39–57.
[21] S.I. Kundalwal, M.C. Ray, Estimation of thermal conductivities of a novel fuzzy fiber reinforced composite, Int. J. Therm. Sci. 76 (2014) 90–100.
[22] G. Chatzigeorgiou, G.D. Seidel, D.C. Lagoudas, Effective mechanical properties of "fuzzy fiber" composites, Compos. B Eng. 43 (2012) 2577–2593.
[23] I. Tsukrov, B. Drach, Elastic deformation of composite cylinders with cylindrically orthotropic layers, Int. J. Solid Struct. 47 (2010) 25–33.
[24] Q. Chen, G. Wang, M.-J. Pindera, Homogenization and localization of nanoporous composites-A critical review and new developments, Compos. B Eng. 155 (2018) 329–368.
[25] Y. Rao, J. Ban, S. Yao, K. Wang, N. Wei, Y. Lu, S. Ahzi, A hierarchical prediction scheme for effective properties of fuzzy fiber reinforced composites with two-scale interphases: based on three-phase bridging model, Mech. Mater. 152 (2021) 103653.
[26] Z.-M. Huang, L.-s. Wang, F. Jiang, Y.D. Xue, Detection on matrix induced composite failures, Compos. Sci. Technol. 205 (2021) 108670.
[27] Z.-M. Huang, A bridging model prediction of the ultimate strength of composite laminates subjected to biaxial loads, Compos. Sci. Technol. 64 (2004) 395–448.
[28] R. Malekimoghadam, U. Icardi, Prediction of mechanical properties of carbon nanotube–carbon fiber reinforced hybrid composites using multi-scale finite element modelling, Compos. B Eng. 177 (2019) 107405.
[29] G. Chatzigeorgiou, Y. Efendiev, D.C. Lagoudas, Homogenization of aligned "fuzzy fiber" composites, Int. J. Solid Struct. 48 (2011) 2668–2680.
[30] X. Ren, J. Burton, G.D. Seidel, K. Lafdi, Computational multiscale modeling and characterization of piezoresistivity in fuzzy fiber reinforced polymer composites, Int. J. Solid Struct. 54 (2015) 121–134.
[31] Q. Chen, M.-J. Pindera, Homogenization and localization of elastic-plastic nanoporous materials with Gurtin-Murdoch interfaces: an assessment of computational approaches, Int. J. Plast. 124 (2020) 42–70.
[32] Q. Chen, J. Zhu, W. Tu, G. Wang, A tangent finite-volume direct averaging micromechanics framework for elastoplastic porous materials: theory and validation, Int. J. Plast. 139 (2021) 102968.
[33] Z. He, M.-J. Pindera, Finite volume based asymptotic homogenization theory for periodic materials under anti-plane shear, Eur. J. Mech. Solid. 85 (2021) 104122.
[34] G. Chatzigeorgiou, N. Charalambakis, Y. Chemisky, F. Meraghni, Periodic homogenization for fully coupled thermomechanical modeling of dissipative generalized standard materials, Int. J. Plast. 81 (2016) 18–39.
[35] E. Tikarrouchine, A. Benaarbia, G. Chatzigeorgiou, F. Meraghni, Non-linear FE2 multiscale simulation of damage, micro and macroscopic strains in polyamide 66-woven composite structures: analysis and experimental validation, Compos. Struct. 255 (2021) 112926.
[36] Q. Chen, G. Wang, X. Chen, J. Geng, Finite-volume homogenization of elastic/viscoelastic periodic materials, Compos. Struct. 182 (2017) 457–470.
[37] D. Chatziathanasiou, Y. Chemisky, G. Chatzigeorgiou, F. Meraghni, Modeling of coupled phase transformation and reorientation in shape memory alloys under non-proportional thermomechanical loading, Int. J. Plast. 82 (2016) 192–224.
[38] E. Pruchnicki, Hyperelastic homogenized law for reinforced elastomer at finite strain with edge effects, Acta Mech. 129 (1998) 139–162.
[39] S.I. Kundalwal, M.C. Ray, Effective properties of a novel continuous fuzzy-fiber reinforced composite using the method of cells and the finite element method, Eur. J. Mech. Solid. 36 (2012) 191–203.
[40] Z. He, M.-J. Pindera, Locally exact asymptotic homogenization of viscoelastic composites under anti-plane shear loading, Mech. Mater. 155 (2021) 103752.
[41] A.S. Drago, M.-J. Pindera, A locally exact homogenization theory for periodic microstructures with isotropic phases, J. Appl. Mech. (2008) 75.
[42] S. Yin, Z. He, M.-J. Pindera, A new hybrid homogenization theory for periodic composites with random fiber distributions, Compos. Struct. 269 (2021) 113997.
[43] S. Gajek, M. Schneider, T. Böhlke, An FE–DMN method for the multiscale analysis of short fiber reinforced plastic components, Comput. Methods Appl. Mech. Eng. 384 (2021) 113952.
[44] S. Gajek, M. Schneider, T. Böhlke, On the micromechanics of deep material networks, J. Mech. Phys. Solid. 142 (2020) 103984.
[45] D. Tsalis, G. Chatzigeorgiou, N. Charalambakis, Homogenization of structures with generalized periodicity, Compos. B Eng. 43 (2012) 2495–2512.
[46] D. Tsalis, T. Baxevanis, G. Chatzigeorgiou, N. Charalambakis, Homogenization of elastoplastic composites with generalized periodicity in the microstructure, Int. J. Plast. 51 (2013) 161–187.
[47] H. Yang, W.H. Müller, Size effects of mechanical metamaterials: a computational study based on a second-order asymptotic homogenization method, Arch. Appl. Mech. 91 (2021) 1037–1053.
[48] H. Yang, B.E. Abali, D. Timofeev, W.H. Müller, Determination of metamaterial parameters by means of a homogenization approach based on asymptotic analysis, Continuum Mech. Therm. 32 (2020) 1251–1270.
[49] G.J. Dvorak, Transformation field analysis of inelastic composite materials, Proc. Roy. Soc. Lond. Math. Phys. Sci. 437 (1992) 311–327.
[50] G. Chatzigeorgiou, N. Charalambakis, Y. Chemisky, F. Meraghni, Thermomechanical Behavior of Dissipative Composite Materials, Elsevier, 2018.
[51] N.M.A. Nik Long, A.A. Khaldjigitov, U. Adambaev, On the constitutive relations for isotropic and transversely isotropic materials, Appl. Math. Model. 37 (2013) 7726–7740.
[52] M. Krause, T. Böhlke, Maximum-entropy based estimates of stress and strain in thermoelastic random heterogeneous materials, J. Elasticity 141 (2020) 321–348.